

# A Customizable, Low-Cost Alternative for Distributed 2D Flow Sensing in Swarms

Jack A. Defay, Jacob M. Peters, and Kirstin Petersen

Electrical and Computer Engineering, Cornell University, Ithaca NY-14853, USA  
jad452@cornell.edu, jmp547@cornell.edu, kirstin@cornell.edu

**Abstract.** Many collective behaviors in social insects are mediated by airflow such as honeybees fanning their wings to drive nest ventilation or to disperse pheromones during olfactory search and aggregation. Empirical investigations of how the local sensing and actuation of individual insects scale up to produce such large scale flows require distributed flow measurement techniques. Common vision-based techniques are not workable in the cluttered dynamic environments in which these social insects live and behave. Here, we develop a customizable, low-cost 2D flow sensor that can measure both magnitude and direction and be deployed in dense sensor arrays on experimental surfaces. While many 2D thermal flow sensor designs have been published, our minimal design uses off-the-shelf components and standard fabrication techniques that should be accessible to most research groups. Here we report on the design and performance of our sensor and provide a calibration protocol that can be implemented by the user. The sensor has a measurement range of 0-2 m/s with accuracy of 0.1 m/s, angular resolution of  $15^\circ$ , and a time constant of 3 s. We also discuss modifications that can be made to tune sensor performance for a given application.

**Keywords:** Social Insects, Flow Sensing, Field Instruments

## 1 Introduction

Social insects coordinate collective behaviors through interactions among individuals which sense and modify their local environment. This phenomenon is especially apparent in termite and ant nest construction where extraction and deposition of material in the environment by one individual informs the behavior of others [1]; techniques which have also inspired numerous multi-robot systems [2]. In some cases, coordination arises from distributed interactions with dynamic media, such as airflow, rather than static media. For instance, some termites and ants build and continuously remodel their nests to promote ventilation, and honeybees drive airflow through wing-fanning to drive nest ventilation or to disperse pheromones during olfactory search and aggregation [3,4,5]. Insights on such flow-mediated coordination can inspire radically new robot coordination algorithms. Empirical study of how the local sensing and actuation of individual insects scale up to produce large scale flows requires distributed flow measurement techniques in cluttered environments in which vision-based flow measurements (e.g., particle image velocimetry) fail. Therefore, we developed a customizable, 2D flow sensor that can be deployed in dense arrays to quantify the flow that is sensed and/or driven by social insects.

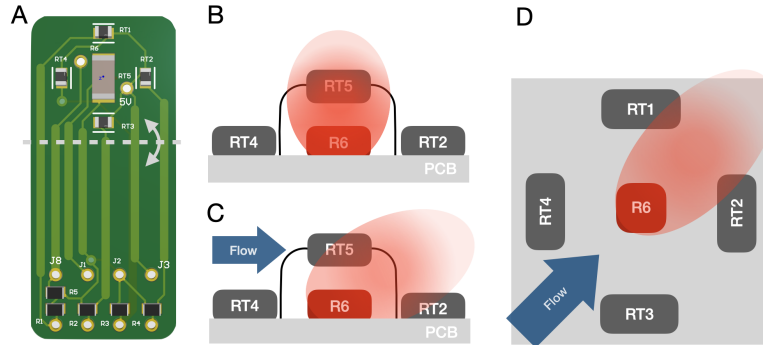


Fig. 1: (A) Sensor PCB. The dashed line indicates a fold line. Four thermistors (RT1-4) surround a heated resistor (R6); an additional through-hole thermistor (RT5) is suspended directly above R6. (B) At zero airspeed, the heat generated by R6 rises straight up to heat RT5. (C,D) At higher airspeeds, the heat is biased towards a subset of RT1-RT4 which indicates the direction of airflow.

Traditional hotwire anemometers are relatively expensive (hundreds of USD) and measure only flow speed, not direction. Microflows are suitable only for 1D applications such as flow measurement in tubes, e.g. used to measure ventilatory flows in termite mounds [6]. Many 2D thermal flow sensors have been published in the last few decades [7,8,9,10,11,12,13,14]. Most of them involve heating elements surrounded by multiple temperature sensors [11], which permit sensing of both magnitude and direction of the airflow along the sensor surface. However, these sensors are produced with micro-machining or lamination techniques that are inaccessible to nonspecialists and often require complex processing or machine learning to interpret the output [12].

We took inspiration from these sensors, but optimized our design for measurements of directional flows in relation to social insects, including: 1) small and symmetric form factor to minimally affect the existing airflow and insect behavior; 2) robustness to insect interaction; 3) low thermal capacity to support higher temporal resolution; 4) low cost to support large numbers; 5) simple fabrication, customization, and calibration that does not require specialized equipment or know-how; and 6) simple data analysis that can run on commodity computers without specialized software. Our design uses a flexible printed circuit board (PCB) with one central heating element surrounded by 5 thermistors (Fig. 1). Our approach achieves reasonable accuracy of 0.1 m/s, resolution down to 0.3 m/s and  $15^\circ$ , and a time constant of 3 s. The design uses standard PCB fabrication, few components, requires less than 2 hours of assembly time, and cost only 13.75 USD, although bulk pricing can reduce the price total substantially. We report on the design and performance of our sensor, detail a calibration protocol that can be implemented by any user in a standard laboratory, and suggest easy customization to suit particular applications. All design files are available open source (<https://github.com/CEI-lab/Scalable2DFlowSensor/>).

## 2 Design and Fabrication

Towards a small, symmetric form factor with low thermal capacity, we implemented the entire sensor on a flexible PCB (Fig. 1A) that can fold along a flexure line such that only the sensing components are exposed and the remainder can be slotted through the experimental surface where it can be accessed and wired from below. We ordered these PCBs from OSHpark at 3.66 USD per piece.

The sensor is composed of a heating element surrounded by 4 thermistors to measure the direction of the airflow and an additional thermistor suspended above the heating element by 2 mm to measure airspeed (Fig. 1B-D). We chose to decouple these measurements in hardware, rather than software as has been shown in related work, to thermally isolate the sensor from the PCB. This improves response time and simplifies data analysis. Our heating element is a  $100\Omega$  2W 2010 surface mount (SMD) power resistor from TE Connectivity. This resistor acts as a resistive heater run in constant power (CP) mode, approximated by a constant input voltage, similar to the system shown in [15]. The 4 surrounding  $10k\Omega$  0805 SMD thermistors are from Vishay. The last  $10k\Omega$  through-hole thermistor is from TDK Electronics (B57541G1103F000).

The thermistors are coupled in series with fixed resistors such that their output can be read using a simple Analog to Digital Converter (ADC). For larger arrays, multiple sensors can be coupled to any embedded processor with a multi-channel ADC as is common e.g. in the popular Arduino platforms. We converted the sensor output,  $V_{out}$ , to airspeed using a linearly interpolated lookup table obtained from our calibration curve. To measure airflow direction, we used the Arduino Mega which is capable of differential amplification and conversion. Specifically, we measured differential inputs from opposing (North-South, East-West) thermistors, similar to a Wheatstone Bridge configuration,  $\delta V_{out}^{NS}$  and  $\delta V_{out}^{EW}$ , and used simple trigonometry to compute the angle of the airflow:

$$\phi = \arctan \frac{\delta V_{out}^{NS}}{\delta V_{out}^{EW}} \quad (1)$$

## 3 Wind Tunnel Design for Sensor Calibration

In lieu of more advanced equipment, we detail two simple wind tunnel designs made with readily accessible components for calibrating the magnitude sensor (Fig. 2A-B). The first produces flow up to 2 m/s, the other up to 5.5 m/s. Our design balances constraints of expense, airspeed range, and laminar flow.

The slow wind tunnel consists of a main stage ( $140 \times 140 \times 600 \text{ mm}^3$ ) with a computer fan (213 cfm, Wathai B07SGWNV5J) drawing air out from the tunnel at one end, and a straw-based laminarizer at the other end. The faster wind tunnel has the same length, but a smaller cross-section ( $50 \times 50 \text{ mm}^2$ ) and an additional settling chamber and linear compression stage ( $140 \times 140 \times 254 \text{ mm}^3$ ) mounted before the fan. To induce laminar flow, we use a long main stage, a  $10^\circ$  compression stage transition angle, and a straw length to diameter ratio of 10. The tunnels were made out of cardboard with a slot near the floor to insert the sensors. The straws were kept in place by a plastic wire mesh, and we found

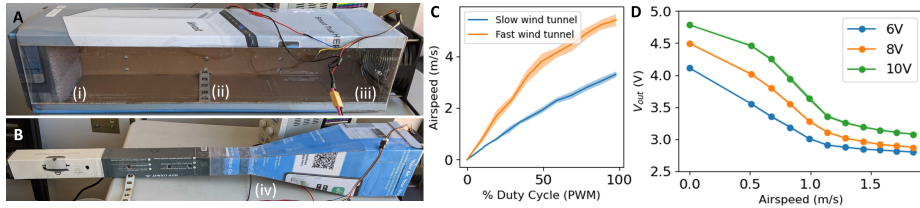


Fig. 2: (A) Windtunnel with airspeeds of 0-2 m/s with a straw-based laminarizer (i), a sensor (ii), and a fan (iii). (B) Windtunnel with compression stage (iv) and airspeeds of 5.5 m/s. (C) Calibration curves for the windtunnels. The x-axis shows the fan duty cycle, the y-axis shows the airspeed measured by a commercial anemometer (TSI 9535 Velocicalc Digital Air Velocity Meter). The solid line denotes the average over 60 s (600 samples) and the shaded region shows the standard error. (D) Magnitude calibration curve at different driving voltages.

that additional layers of mesh could be added to extend the lower range of active airspeeds below 0.5 m/s. We also added an optional viewing window along the side of the tunnel made of acrylic.

We characterized the wind tunnel using a reference anemometer (Fig. 2C) and then used the wind tunnel to calibrate our sensors. We found a low average error across the range of airspeeds indicating mostly laminar flow. To calibrate the magnitude sensor, we ran the fan at various duty cycles in 60 s intervals while recording  $V_{out}$ . Fig. 2D shows calibration data for three different supply voltages across the power resistor.

## 4 Sensor Characterization

To characterize the sensor, we considered four key metrics: accuracy, range, measurement resolution, and temporal resolution. The range of the magnitude sensor is shown in Fig. 2D as a function of the heating element supply voltage. We found that at speeds greater than 2 m/s, the noise in the signal made the readings indistinguishable. Fig. 3A shows a step response test from 0-2 m/s to characterize the magnitude sensor’s time constant. Upon heating, the sensor has a 90% rise time,  $T_{0.9}^{mag} = 11.00$  s, and reaches 63.2% of its final value in  $\tau^{mag} = 3.01$  s. Upon cooling (going from higher to lower airspeed) the time constant is slightly slower: 13.76 s and 6.16 s, respectively. We find the accuracy of the magnitude sensor at steady state by subtracting the calibrated sensor value from known airspeed, for an average and standard deviation error of  $0.11 \pm 0.01$  m/s. To find the sensor resolution, we repeated the step response for incrementally smaller step values (Fig. 3B), starting at the middle of the sensor range (1.14 m/s). We consider the minimum resolution to be at the point when the standard deviation at steady state before and during the step overlaps. With a moving average similar to our time constant ( $t_{avg} = 3$  s), the resolution is 0.25 m/s. At  $t_{avg} = 10$  s the resolution improves to 0.1 m/s at the cost of a slower response. In comparison, the  $\sim$ 1K USD anemometer used to calibrate the wind tunnel has a time constant of 1 s and a resolution of 0.01 m/s.

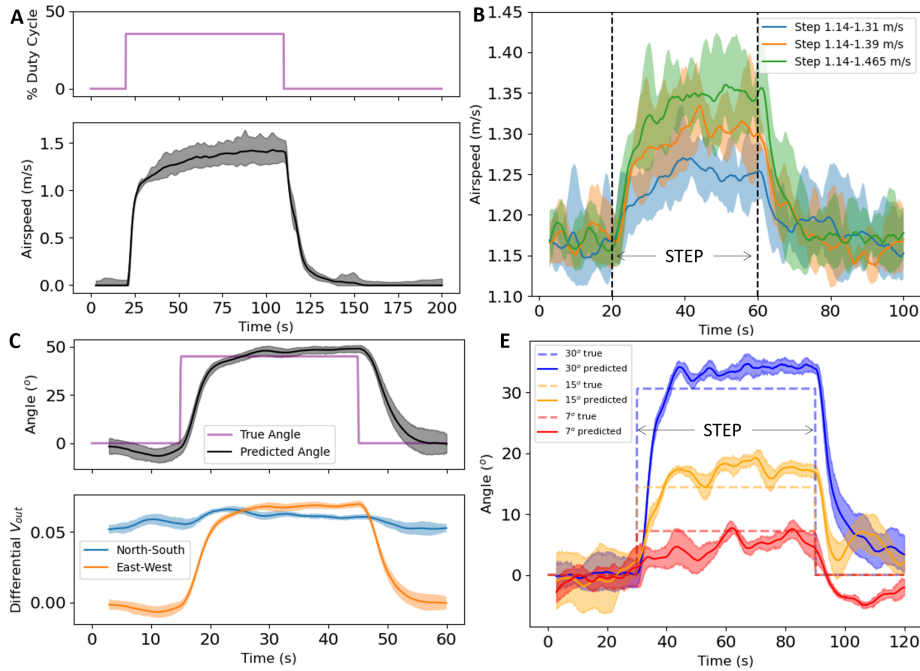


Fig. 3: A) Example of a step performed in the wind tunnel, with corresponding response from the magnitude thermistor (RT5). B) Step response performed to determine sensor resolution near the middle of its absolute range (1.14 m/s). Each trial was collected using a 3 s moving average filter. Solid line shows average; shaded region shows standard deviation. C) Computed (top) and raw (bottom) sensor output on angular step response. D) Angular step response to determine directional resolution, set up similar to (C). All experiments were done with 8 V supply.

To characterize the directional sensor, we performed similar step response tests (Fig. 3C-D), but with angle. We found  $\tau^{dir} = 4.3$  s and the measurement resolution to be  $15^\circ$  with  $t_{avg} = 3$  s. At 1.14 m/s airspeed, we found the average and standard deviation error to be  $3.88 \pm 0.30^\circ$ . We expect that better tuning of the wind tunnel for laminar flow, suppression of 60 Hz interference, and increased differential amplification may improve these numbers.

In Table 1 we compare the performance of this sensor to other 2D sensors reported in literature.

## 5 Customization

The inherent advantage of the minimalistic design we present here is the ease of customization for different applications. Next, we discuss potential parameters to be changed and how these trade off sensor performance.

There are several ways to change the sensor response time to fit the particular signal to be measured. The sensor is based on a flexible PCB, which is thin, has

Table 1: Key aspects of our sensor compared to other custom sensors in literature. Note that characterization techniques differ between papers.

Reference	Range	Magnitude		Direction		Manufacturing
		Accuracy	Resolution	Accuracy	Resolution	
This paper	2 m/s	0.1 m/s	0.25 m/s	4°	15°	Std. soldering
[8]	30 m/s	0.65 m/s	NA	0.96°	NA	MEMS
[10]	40 m/s	0.5 m/s	NA	2°	NA	MEMS
[11]	33 m/s	0.33 m/s	0.04 m/s	1.5°	1°	MEMS
[14]	37 m/s	0.5 m/s	NA	2.7°	NA	MEMS
[16]	10 m/s	0.36 m/s	NA	1.2°	NA	MEMS

low thermal mass, and can sit flush with the experimental surface. Flexible PCBs, however, are also more fragile. We found that sensors implemented on stiff 0.8 mm PCB are more robust, but also react slower and transmit the heat over a larger surface which may deter close operation with insects. The thermistors used in our sensor have a thermal mass that is dependent on the size of the glass bead which surrounds the sensor. We tested a larger bead size (MF58, Uxcell) and found that the small thermistor bead was more responsive and pick up higher frequency fluctuations while the large thermistor bead have a slower response time; specifically, we measured the rise time constant in this setup to be 11.6 s.

To change the absolute range of the sensor, the user can change the the distance of the thermistors to the heating element and the size of the thermistor bead. Another easier modification is to increase the range by increasing the supply voltage for the heating element (R6) at the cost of increased temperature, which may negatively affect nearby insects. Note that excessive heating above 150°C may also negatively affect the life time of the sensor.

To demonstrate the versatility of our approach, we implemented and briefly field-tested two variants. The first variant was designed to better withstand direct insect interactions. We extended the flexible PCB, folding it over three times to produce a stable rectangular cross-section. The roof of this cross-section was slotted as to not hinder airflow. This design permitted us to replace the through-hole thermistor with a cheaper SMD thermistor (Fig. 4A-B). As before, the end of the PCB was slotted through a cavity in the experimental surface. The second variant was a 1D magnitude sensor array with 8 thermistor heating element pairs (Fig. 4C-D). 1D sensing reduced complexity and allowed for more data collection in the brief field season we had.

## 6 Exploratory Field Test

Our design was motivated by the study of olfactory search and aggregation, used in swarm cluster formation and nest entry in honeybees (Fig. 4). This behavior involves coordinated movements, collectively driving pheromone-laden airflow with their wings away from the queen’s position and walking upstream toward her [5]. To study this phenomenon, we needed to measure airflow generated by the honeybees along a cluttered 2D surface.

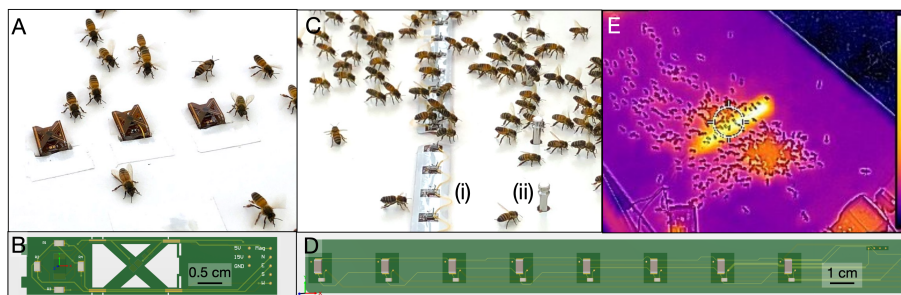


Fig. 4: Examples of our sensors used in biological assays, including a covered sensor (A,B) and a magnitude sensor array (C,D). Note the size of the custom sensors (C.ii.) as compared to the commercial anemometers (C.i.). (D) Thermal image of bees crossing the magnitude sensor array. The bees do not appear to be deterred by the heat generated.

To test the field-readiness of our sensor, we installed two prototypes on a surface to measure the flows induced by honeybees. We placed two of the magnitude sensor arrays (described above) together to make a 16-sensor array perpendicular to the direction of bee/air movement (Fig. 4B). The bees traversed the sensor array while performing typical scent-fanning behavior, enabling biological measurements which will be the subject of future research. We also tested the variant of the 2D flow sensor (Fig. 4A) with the folded housing which prevented the bees from directly contacting the sensing components.

We validated that the sensors were small and low profile enough to not deter honeybees from traversing them (Fig. 4A,C) and that the heating elements produced enough heat ( $\sim 87^{\circ}\text{C}$ ) to sense effectively from 0-2 m/s, but not enough to deter nearby honeybees (Fig. 4E). While some characteristics of our sensor were sufficient for our study (i.e., 0.25 m/s resolution;  $15^{\circ}$  angular resolution, 3 s time constant), the peak airspeed generated by the bees exceeded the 2 m/s limit of our sensor. In future iterations, we intend to increase the range of our sensor by tuning the proximity of the magnitude thermistor to the heating element.

## 7 Conclusion

In brief, we presented a simple method to create and calibrate low cost 2D flow sensors. Although the sensors cannot compare in performance to those made with more complex manufacturing techniques, they lend themselves to easy customization for large scale deployment with social insects. This work to create accessible technology is an important step in the process of uncovering how social insects sense, manipulate, and coordinate through airflow.

## Acknowledgements

This work was supported by an NSF Award (#1739671), a Cornell LSAMP Award, and the Packard Fellowship for Science and Engineering.

## References

1. A. Perna and G. Theraulaz, “When social behaviour is moulded in clay: on growth and form of social insect nests,” *The Journal of Experimental Biology*, vol. 220, no. 1, pp. 83–91, 2017.
2. K. Petersen and R. Nagpal, “Complex design by simple robots: A collective embodied intelligence approach to construction,” *Architectural Design*, vol. 87, no. 4, pp. 44–49, 2017.
3. J. M. Peters, N. Gravish, and S. A. Combes, “Wings as impellers: honey bees co-opt flight system to induce nest ventilation and disperse pheromones,” *Journal of Experimental Biology*, vol. 220, no. 12, pp. 2203–2209, 2017.
4. J. M. Peters, O. Peleg, and L. Mahadevan, “Collective ventilation in honeybee nests,” *Journal of The Royal Society Interface*, vol. 16, no. 150, p. 20180561, 2019.
5. J. M. Peters and K. H. Petersen, “Honeybee swarms use a flow-mediated pheromone signaling scheme to coordinate aggregation,” in *SICB*, vol. 60, 2020, pp. E185–E185.
6. H. King, S. Ocko, and L. Mahadevan, “Termite mounds harness diurnal temperature oscillations for ventilation,” *Proceedings of the National Academy of Sciences*, vol. 112, no. 37, pp. 11 589–11 593, 2015.
7. Y. Zhu, B. Chen, M. Qin, and Q. Huang, “2-D Micromachined Thermal Wind Sensors—A Review,” *IEEE Internet of Things Journal*, vol. 1, no. 3, pp. 216–232, 2014.
8. R. Que and R. Zhu, “A Compact Flexible Thermal Flow Sensor for Detecting Two-Dimensional Flow Vector,” *IEEE Sensors Journal*, vol. 15, no. 3, pp. 1931–1936, 2015.
9. R. Zhu, R. Que, and P. Liu, “Flexible micro flow sensor for micro aerial vehicles,” *Frontiers of Mechanical Engineering*, vol. 12, no. 4, pp. 539–545, 2017.
10. S. Wang, Z. Yi, M. Qin, and Q. Huang, “A 2d wind sensor using the p thermal feedback Control,” *Journal of Microelectromechanical Systems*, vol. 27, no. 3, pp. 377–379, 2018.
11. Y. Ye, Z. Yi, S. Gao, M. Qin, and Q. Huang, “Octagon-shaped 2-d micromachined thermal wind sensor for high-accurate applications,” *Journal of Microelectromechanical Systems*, vol. 27, no. 4, pp. 739–747, 2018.
12. D. Barmpakos, I. T. Famelis, A. Moschos, D. Marinatos, and G. Kaltsas, “Design and Evaluation of a Multidirectional Thermal Flow Sensor on Flexible Substrate,” *Journal of Sensors*, vol. 2019, p. e8476489, 2019.
13. S. Gao, Z. Yi, Y. Ye, M. Qin, and Q. Huang, “Temperature Effect and Its Compensation of a Micromachined 2-D Anemometer,” *IEEE Sensors Journal*, vol. 19, no. 14, pp. 5454–5459, 2019.
14. Y. Lan, Y. Zou, X. Ma, Y. Shi, J. Fan, Y. Hai, X. Wang, J. Yang, and Q. Feng, “Fabrication and Characterization of Dual Coordinate Self Examined Thermal Flow Sensor Arrays Based on Longitudinal Heat Conduction,” *IEEE Sensors Journal*, vol. 20, no. 1, pp. 434–440, 2020.
15. G. Shen, M. Qin, and Q. Huang, “A Cross-Type Thermal Wind Sensor With Self-Testing Function,” *IEEE Sensors Journal*, vol. 10, no. 2, pp. 340–346, 2010.
16. H. Liu, N. Lin, S. Pan, J. Miao, and L. K. Norford, “High Sensitivity, Miniature, Full 2-D Anemometer Based on MEMS Hot-Film Sensors,” *IEEE Sensors Journal*, vol. 13, no. 5, pp. 1914–1920, 2013.